# In Situ Functionalization of Stable 3D Nest-Like Networks in Confined Channels for Microfluidic Enrichment and Detection

*Gang Wang, Guoying Shi, Hongzhi Wang,* Qinghong Zhang, and Yaogang Li**

**Construction of stable 3D networks directly on the inner wall of microchannels is of great importance for various microfluidic applications. 3D nest-like networks with large contact surface areas and excellent structural stability are fabricated via a facile, template-free, continuous fluid construction process directly in confined microchannels. Bovine serum albumin (BSA) is chosen as a model albumin to test the adsorption of the network modified microchannel to the target albumin. The high structural stability of the networks is confirmed both by finite element analysis (FEA) simulation and recycling experiments for BSA enrichment. ZnS shells are fabricated based on the original 3D Zn(OH)F networks through in situ chemical conversion. The nest-like networks decorated with Ag nanoparticles (NPs) serve as 3D substrates for surface-enhanced Raman scattering (SERS), exhibiting excellent sensitivity for rapid detection of trace $10^{-12}$ mol $L^{-1}$ (1 pM) BSA. Three different gap sizes between Ag NPs in the 3D geometry create a large number of SERS hot spots that contribute to the high sensitivity of the networks. Furthermore, a transparent, flexible, microfluidic device containing the 3D nest-like structures exhibits excellent recyclability and flexible stability for trace BSA enrichment, showing potential for application in online SERS detection.**

## 1. Introduction

Microfluidic systems, in which fluids are controlled and analyzed within microscale channels, have received intense interest from both industrial and academic communities.[1] The benefits of miniaturization, integration, and automation have prompted their use in various applications ranging from materials synthesis,[2] energy harvesting,[3] point-of-care diagnostics,[4] to biomolecule filtration and capture.[5] In many of these applications, micro/nanostructures built in the microchannels influence the overall performances of microfluidic systems. For example, built-in micro/nanostructures are important in mixing, cell studies, and separation columns.[6] Furthermore, specific topographical morphology leads to specific functionality.[7] Various micro/nanostructures (e.g., microcolumns, microneedles, nanowires) have been prepared to separate biological components including rare circulating tumor cells, DNA, and viruses.[5a,8] However, the traditional micro/nanostructures situated in microchannels are mainly fabricated by expensive, sophisticated processes such as microelectromechanical system techniques, laser machining, micromechanical machining and ink jet printing. The obtained structures also suffer from some limitations in elaborate regulation, especially on scales less than 100 nm.

As a result, chemical fabrication has emerged as a simple convenient method to form structures in microchannels. We have previously demonstrated wet chemical methods to fabricate NPs and nanorods on the inner walls of microchannels.[9] However, these methods cannot achieve sufficient contact surface area, and structural stability is limited. Hence, the integration of 3D networks into microfluidic systems is becoming increasingly important to enhance their effective contact surface area and structural stability. Several strategies have been used to generate 3D network structures.[5a,10] Lee and co-workers suspended 3D single-walled nanotube structures in microchannels by thermal chemical vapor deposition combined with photolithography to develop a new type of microfluidic platform.[5b] Jamal et al. reported the self-assembly of 3D photopatterned polymers embedded in microfluidic channels.[10c] It should be noted that the tethering of 3D networks described above is exclusively accomplished via an open-surface approach; that is, micro/nanostructure fabrication must be achieved prior to its integration. Such off-site modification is rather tedious, and most importantly, the integration process will damage micro/nanostructures fabricated in the

Dr. G. Wang, Prof. H. Z. Wang, Prof. Q. H. Zhang
State Key Laboratory for Modification of Chemical Fibers and Polymer Materials
College of Material Science and Engineering
Donghua University
Shanghai, 201620, China
E-mail: wanghz@dhu.edu.cn
G. Y. Shi
College of Chemistry
Chemical Engineering and Biotechnology
Donghua University
Shanghai, 201620, China
Prof. Y. G. Li
Engineering Research Center of Advanced Glasses Manufacturing Technology, MOE
Donghua University
Shanghai, 201620, China
E-mail: yaogang_li@dhu.edu.cn

**DOI: 10.1002/adfm.201301936**

microchannels. The in situ fabrication of a stable 3D structure in a closed-surface channel system has not been reported. This suggests direct fabrication of 3D networks with large surface area and good structural stability in confined microchannels via facile methods is difficult. However, construction of stable 3D networks directly on the inner wall of microchannels is of great importance for various microfluidic applications, so it should be attempted.

The micro/nanostructures in microchannels need to possess functional surfaces for biomolecule (blood cell, bacteria, virus and protein) enrichment and detection.[11] Such functionalization is mainly achieved by grafting specific biomolecules on the surface of substrates via electrostatic bonding. However, the functional surface formed by this method has relatively low structural and chemical stability, especially toward fluid erosion in microfluidic applications. Generating core/shell structures with structural and chemical stability in situ on the inner walls of microchannels by wet chemical methods is a new strategy to fabricate functionalized microfluidic devices.[12] In addition, surface-coating of a 3D stable network by in situ chemical conversion can not only enhance stability because chemical bonding is used rather than electrostatic, but also provide support for further modification with other functional groups, and thus offer potential for many more functionalities to be introduced. Therefore, in situ chemical conversion to form a functionalized shell via chemical bonding onto a substrate surface followed by formation of surface specific-group electrostatic interactions will be a novel approach to realize surface functionalization in confined microchannels, which is important for microfluidic applications.

The integration of active SERS substrates into microfluidic device has been developed rapidly for its tremendous potentials in chemical and biological sensing applications due to its high sensitivity, rapid response, and low dosage.[13] For instance, Lee et al. reported a flexible integration fabrication of SERS-based immunoassay using a gold array-embedded gradient microfluidic chip.[14] Choo et al. used silver colloids as reproducible SERS substrates for detection of DNA in an alligator teeth-shaped microfluidic channel.[15] The above substrates were found to provide highly sensitive detection. Despite the fact that SERS substrates are successfully adopted by microfluidic systems, there are still a lot of problems in compatibility, reproductivity and accuracy in real microfluidic analysis. The most important reason is that optical scattering and light collection occur in a three dimensional focal volume.[16] To maximize the quantity of the scattered light generated and detected, SERS substrates should contain hot spots in a large three dimensional volume. Therefore, it is desirable to integrate 3D composites SERS substrates with the microchannels to form plentiful hot spots for highly sensitive detection activity.

Herein, 3D nest-like networks with large surface area and excellent structural stability were fabricated directly in confined microchannels using a facile, template-free, continuous fluid construction process. Furthermore, a functional surface coating was produced by in situ chemical conversion on the original networks to enhance its specific interactions with biomolecules. BSA was chosen as a model albumin and used to test the protein adsorption and SERS detection ability of these networks.

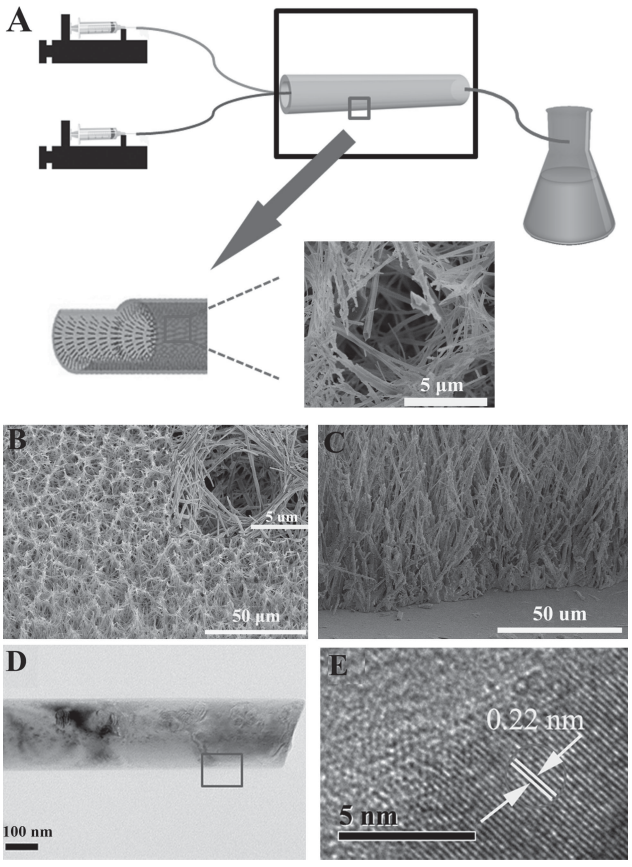


**Figure 1.** A) Schematic of the experimental system; B) Typical FE-SEM image of tilted view of networks (the inset is the corresponding highly magnified image); C) Typical FE-SEM image of cross-sectional view of networks grown on the inner wall; D) TEM image; and E) HRTEM image of pristine networks on the inner wall of a microchannel.

The integration of Ag NPs decorated nest-like networks into the microfluidic channels acted as 3D SERS substrates, which exhibited excellent sensitivity for rapid microfluidic detection of trace biomolecules owing to three kinds of hot spots in a large 3D volume.

## 2. Results and Discussion

### 2.1. Structure and Morphology

#### *2.1.1. Zn(OH)F Nest-Like Networks*

The nest-like networks were obtained by continuous fluid construction with two kinds of reaction fluid flowing through the microchannels, just as **Figure 1**A shows. As the reaction time and the amount of continuous flow reaction fluid increase, the Zn(OH)F nanorod interlaced with one another and continuous growth of the cross-linked nanowire structure leads to the final nest-like network, detailed formation mechanism of the network was discussed in the Supporting Information (Figures S1, 2). Field emission scanning electronic microscope (FE-SEM) images of pristine Zn(OH)F nest-like networks on

the inner walls of microchannels were shown in Figure 1B,C. The 3D nest-like networks contained numerous micro- and nanosized pores. The structural units linked with each other to form a stable network with large specific surface area. From Figure 1C (the cross section of the networks), we can see that there existed good connection of the network with microchannels. The energy-dispersive X-ray (EDX) spectrum (Figure S3A, Supporting Information) of the networks showed the presence of Zn, O, and F, suggesting the network consisted of Zn(OH)F. Transmission electron microscope (TEM) and high-resolution transmission electron microscope (HRTEM) measurements were performed to further investigate the network structures. A TEM image of pristine Zn(OH)F nest-like networks (Figure 1D) revealed that the network structure was composed of nanorods about 200 nm in diameter with a smooth surface. From Figure 1E, the HRTEM image (the magnified image of the boxed area in Figure 1D) gave further insight into the structural features of the nanorods. The lattice spacing of 0.22 nm between adjacent lattice planes in Figure 1E corresponded to the distance between two (4 1 0) crystal planes of Zn(OH)F, which indicated the successful fabrication of Zn(OH)F. The fluid flow performance through the 3D network-modified microchannels was achieved using Ansys-Fluent software based on the structural model, as shown in Figure S4 (Supporting Information). The finite element analysis (FEA) results theoretically prove the structural stability of the 3D nest-like networks in microchannels; these findings are further corroborated by the following experimental results.

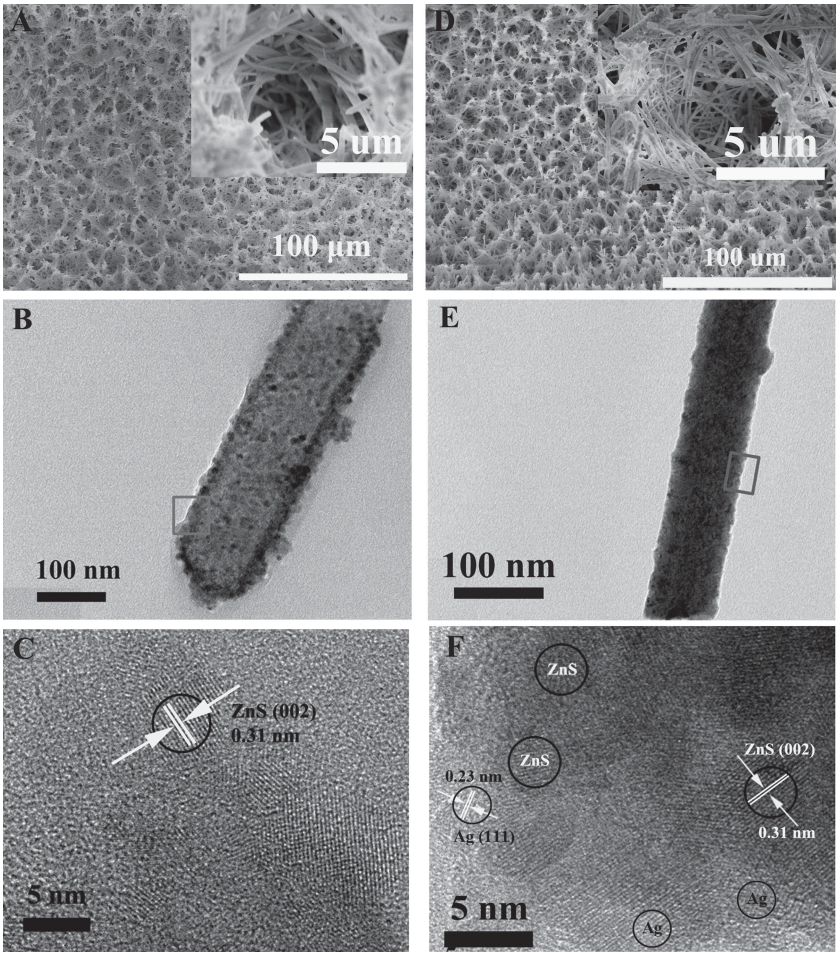


**Figure 2.** A) Typical FE-SEM image (inset shows a magnified image), B) TEM image, and C) HRTEM image of Zn(OH)F@ZnS nest-like networks on the inner wall of a microchannel. D) Typical FE-SEM image (inset shows a magnified image), E) TEM image, and F) HRTEM image of Ag-Zn(OH)F@ZnS nest-like networks on the inner wall of a microchannel.

### *2.1.2. Zn(OH)F@ZnS and Ag-Zn(OH)F@ZnS Nest-Like Networks*

A functional zinc sulfide (ZnS) surface coating was formed via in situ chemical conversion on the original networks to enhance its specific interactions with biomolecules. FE-SEM images of Zn(OH)F@ZnS after 100 min of exposure to thioacetamide (TAA) revealed modified nanorods consisting of the nest-like networks with wrinkled surfaces (**Figure 2**A). An EDX spectrum of these composite networks showed the presence of both Zn and S, suggesting the formation of ZnS (Figure S3B, Supporting Information). TEM and HRTEM measurements were performed to further investigate these structures. In a TEM image of Zn(OH)F@ZnS-2 h, all nanorods showed dark inner centers and relatively lighter edges, indicating a core/shell structure (Figure 2B). From the HRTEM image in Figure 2C (a magnified image of Figure 2B), the calculated interplanar spacing of ~0.31 nm corresponded to the lattice spacing for the (0 0 2) face of wurtzite ZnS. Together, the TEM and EDX results were consistent with the successful formation of Zn(OH)F@ZnS core/shell nanorods. X-ray photoelectron spectroscopy (XPS) analysis also confirmed the successful synthesis of Zn(OH)F@ZnS core/shell nanorods (Figure S5, Supporting Information).

To enhance enrichment efficiency and specific SERS detection performance of the networks, Ag-Zn(OH)F@ZnS nest-like networks were prepared. FE-SEM images of Ag-Zn(OH)F@ZnS nest-like networks on the inner walls of microchannels (Figure 2D) showed that their morphology was similar to that of Zn(OH)F@ZnS nest-like networks. An EDX spectrum of the Ag-modified networks indicated that the composite nanorods consisted of Zn, Ag, and S, suggesting the presence of ZnS and Ag (Figure S3C, Supporting Information). A TEM image of the Ag-Zn(OH)F@ZnS nest-like networks showed the nanorods were covered with dark dots that were ascribed to Ag NPs. An HRTEM image obtained for the rectangular region in Figure 2F showed the shell was polycrystalline. The calculated interplanar spacings of ~0.31 and ~0.23 nm corresponded to lattice spacings for the (002) face of wurtzite ZnS and (111) face of cubic Ag, respectively. The above results together suggested the successful synthesis of Ag-Zn(OH)F@ZnS networks.

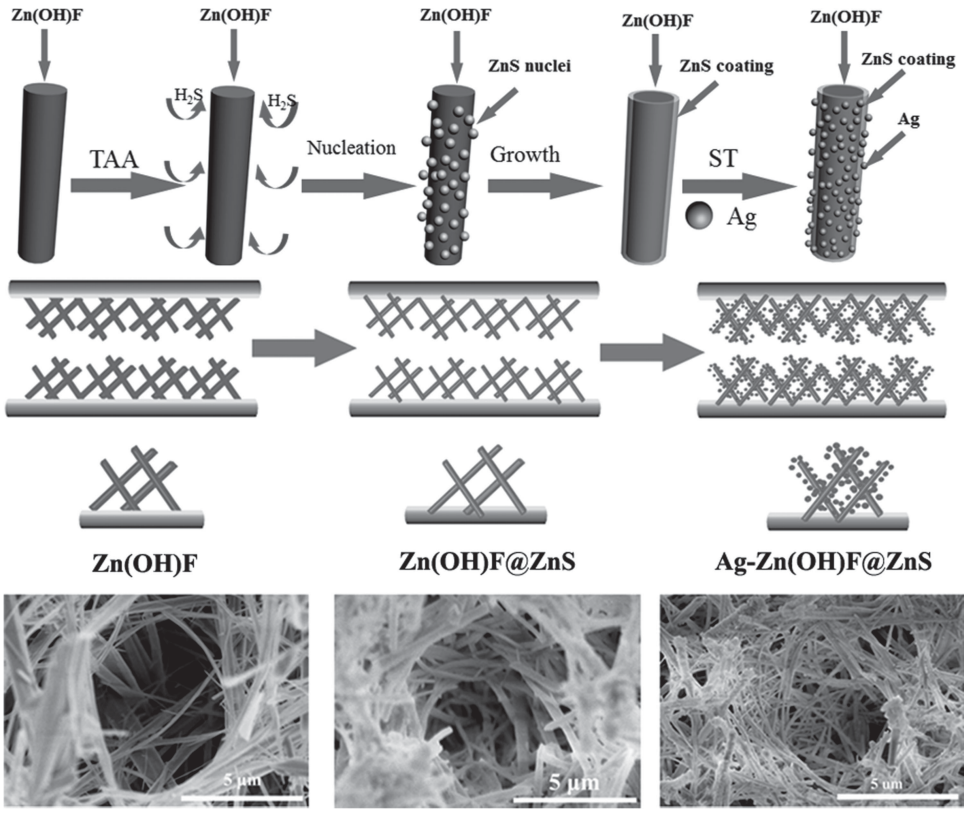


**Figure 3.** Continuous construction of functional nest-like networks on the inner wall of microchannel.

*2.1.3. Proposed Formation Mechanism*

Based on the above results, a formation process for the networks was proposed. A schematic diagram of the process for the continuous construction of multi-layered networks was shown in **Figure 3**. When TAA solution flowed through the microchannels, Zn(OH)F networks in the inner walls of microchannels served as the zinc source and in situ reaction template. TAA solution provided the $S^{2-}$ to react with $Zn^{2+}$ from the Zn(OH)F networks. The lone pair electrons in TAA molecules integrated with empty orbitals of $Zn^{2+}$ to form $ZnHS^+$ coordination compounds, which enhanced the activity of $Zn^{2+}$ in Zn(OH)F networks, facilitating nucleation and growth of ZnS on the surface of the Zn(OH)F networks. The ZnS layer formed while maintaining the original structure of the nest-like network. The following chemical reactions were involved in fabrication of the Zn(OH)F@ZnS networks:

$$Zn^{2+} + CH_3CSNH_2 \leftrightarrow ZnHS^+ + CH_3CSNH^+ \quad (1)$$

$$2ZnHS^+ + S^{2-} \leftrightarrow 2ZnS + H_2S \quad (2)$$

This growth mechanism was also confirmed by XPS analysis of Zn(OH)F@ZnS (Figure S5, Supporting Information). In situ chemical conversion is required to develop functional ZnS surfaces that integrate structure and function with structural and chemical stability. As an effective Ag protecting agent, sodium thioglycolate (ST) has –SH groups on its surface that react with Ag adsorbed on the surface of the network structure to form Ag-S bonds,[17] resulting in Ag-decorated networks (Ag-Zn(OH)F@ZnS). Again, the original nest-like network structure is retained.

## 2.2. Enrichment of BSA Molecules Through the Nest-Like Network-Modified Microchannels

The ability to isolate and manipulate certain biomolecules, such as DNA or protein, from biological matrices opens up a host of potential opportunities for researchers interested in clinical and diagnostic medical science. The separation, determination, and quantification of proteins are basic requisites in clinical medicine, biochemistry, and laboratory tests.[18] BSA was chosen as a model albumin to test the adsorption of the network modified microchannel to the target albumin.The different networks described above were used to capture BSA from 500 μg $mL^{-1}$ BSA solution ($C_0$) while monitoring the BSA concentration at the microchannel exit (C) (**Figure 4**A). Most BSA molecules were adsorbed and retained by the networks in the microchannels, while solvent molecules were flushed away through the channels. With increasing residence time (RT), the ratio of C to $C_0$ gradually decreased, suggesting that the BSA concentration at the microchannel exit decreased.

Comparing the results in Figure 4A, the Zn(OH)F@ZnS and Ag-Zn(OH)F@ZnS networks showed superior BSA capture abilities compared to those of the Zn(OH)F and Ag-Zn(OH)

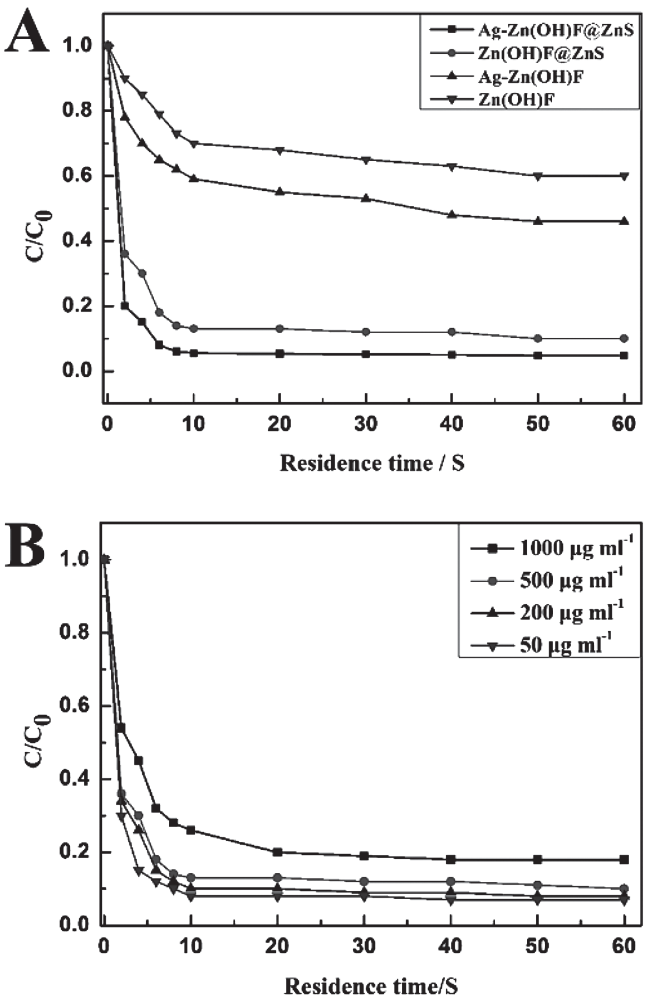


**Figure 4.** A) Adsorption capture of 500 μg $mL^{-1}$ BSA solution with various nest-like network-modified capillary microchannels with different RTs; B) adsorption capture of different BSA concentrations with Zn(OH)F@ZnS network-modified capillary microchannels versus RT.

F networks. The Ag-Zn(OH)F@ZnS networks showed the highest absorption performance with a RT of 10 s, where $C/C_0$ approached 0. Zn(OH)F@ZnS and Ag-Zn(OH)F@ZnS networks demonstrated that superior BSA trapping ability could be achieved by enhanced interactions between networks and BSA molecules caused by the in situ ZnS shells. For the Ag-Zn(OH)F@ZnS networks, the interactions between Ag and BSA also contributed to its high BSA adsorption ability in addition to the above mentioned factors. The above results suggested that the in situ chemical conversion ZnS shells were of great importance in protein enrichment. To further evaluate the ability of the Zn(OH)F@ZnS-modified microchannels to capture BSA, different BSA concentrations were injected through the microchannels. The results showed that the two lowest concentrations of BSA, 200 and 50 μg $mL^{-1}$, were rapidly fully adsorbed with a RT of 6–8 s (Figure 4B). This indicates that the network-modified microchannels show excellent enrichment efficiency for low BSA concentrations similar to those of real biological fluids.

The most important factor in the protein enrichment process for the fabricated structures was the effective contact area with the fluid in confined channels. The micropores in the 3D network reduced fluid resistance, while the nanopores led to nanofluid formation, which greatly enhanced effective fluid contact area of the network. With their large fluid contact area in mind, we investigated the enrichment capacity of the network modified microchannel toward BSA solution. Equivalent length of Zn(OH)F@ZnS networks, ZnO@ZnS nanorod arrays and ZnS nanoparticles modified microchannel were used to enrich BSA molecules; a series of samples using varying amounts of BSAs were prepared. After the samples were loaded, the flow-through fractions were analyzed using UV–vis spectroscopy. When the total amount of BSA was lower than the capacity of the materials, the BSA could not be detected. Once the BSA's signal was detected by UV–vis; meaning that the material could not capture all of the BSAs at the concentration in question; the enrichment capacity of the material could be estimated. As illustrated in **Figure 5**A, the enrichment capacities of ZnS nanoparticles and ZnO@ZnS nanorod arrays modified microchannels were 1800 g $m^{-3}$ and 5850 g $m^{-3}$. Here, 'g $m^{-3}$' represents the adsorption amount in the microchannels with the volume of 1 $m^3$. The Zn(OH)F@ZnS networks modified microchannels showed enrichment capacities as high as 56 700 g $m^{-3}$, nearly 10 times higher than that of ZnO@ZnS nanorod arrays. As detailed above, the Zn(OH)F@ZnS networks modified microchannels featured a large fluid contact area, which ensured the adsorption of the molecules into the networks. And the fast diffusion speed of the fluid in microchannels increase the enrichment speed attributed to the pores in the networks. Also by virtue of the large fluid contact area and fast fluid diffusion, the enrichment could be completed in less than 15 s, nearly 4 times faster that of ZnO@ZnS nanorod arrays, just as illustrated in Figure 5B. From **Figure 6**, these Zn(OH)F@ZnS network-modified microchannels displayed high performance durability to trap BSA multiple times, which further proved the chemical and structural stability of the in situ chemical conversion shells.

### 2.3. SERS Detection of Trace BSA Molecules

To date, protein identification has been performed by various techniques, such as two-dimensional polyacrylamide gel electrophoresis (PAGE), N-terminal sequencing on individual PAGE spots, immunoblotting, and western blotting, all of which require complex operations and are not suitable for determination of trace amounts of proteins.[19] The SERS effect opens up exciting opportunities for the application of vibrational spectroscopy in biology, and makes SERS a promising method in bioanalytics.[20] There are numerous reports that Ag NPs have specific interactions with BSA.[21] Thus, to increase the ability of the modified microchannels to trap and detect low concentrations of BSA, Ag-Zn(OH)F@ZnS network-modified microchannels were used to concentrate BSA and then SERS was employed to detect BSA.

SERS measurements obtained after BSA solution (20 μL, 1 pM) was injected into the Ag-Zn(OH)F@ZnS network and rough Ag substrates modified microchannels exhibited vibrational bands indicative of secondary structure as well as the functional groups of BSA (**Figure 7**A). For the Ag-Zn(OH)F@ZnS network modified microchannel, peaks at 625 and 940 $cm^{-1}$ were attributed to C-C, 1002 $cm^{-1}$ to phenylalanine, 1193 $cm^{-1}$

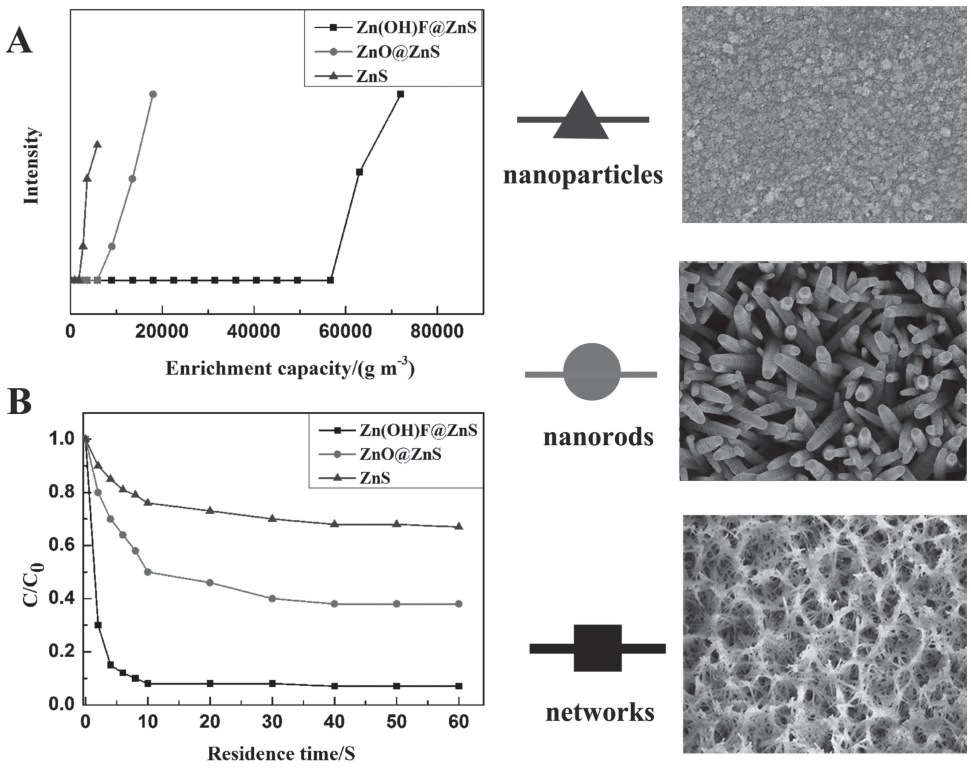


**Figure 5.** A) Enrichment capacity; B) Adsorption capture of 500 μg mL$^{-1}$ BSA solution with different RTs; using Zn(OH)F@ZnS networks, ZnO@ZnS nanorod arrays and ZnS nanoparticles modified capillary microchannels.

to tyrosine, and 1280 cm$^{-1}$ to the amide III region.[22] The band localized at 1559 cm$^{-1}$ was assigned the amide II region, and that at 1600 cm$^{-1}$ to tryptophan/tyrosine/phenylalanine.[22a] The band at 1647 cm$^{-1}$ mainly originated from amide I, and was characteristic of the high α-helical content of BSA.[23] In comparison, only two weak peaks at 1002 and 1647 cm$^{-1}$ could be found in the rough Ag substrates modified microchannel. High intensity bands in the region of 1400–1500 cm$^{-1}$ were mainly attributed to signals from the silica glass capillary microchannel, although they might also have included some BSA vibrational bands. The SERS detection results suggested the high sensitivity of the 3D nest-like network modified channels. The high SERS sensitivity of the Ag-Zn(OH)F@ZnS networks was mainly related to its unique 3D network geometry, as depicted schematically in Figure 7B. Firstly, small Ag NPs were assembled on the surface of the 3D networks via continuous fluid construction to achieve a high density of hot spots in the 3D geometry. The resulting new hybrid 3D substrate showed such high SERS activity that BSA with a concentration as low as 1 pM could still be identified. This is attributed to three gaps of different sizes between the Ag NPs, indicated as 1st, 2nd, and 3rd, form 3D hot spots. 1st were the gaps between the Ag NPs located on the surface of the same nanorod; 2nd were the gaps between the two Ag NPs located on the sides of two neighboring nanorods; and 3rd were the gaps between Ag NPs distributed around the same nanopore in the 3D networks. In summary, three sizes of gaps between Ag nanoparticles in the 3D geometry create a large number of SERS hot spots that contribute to its high sensitivity.

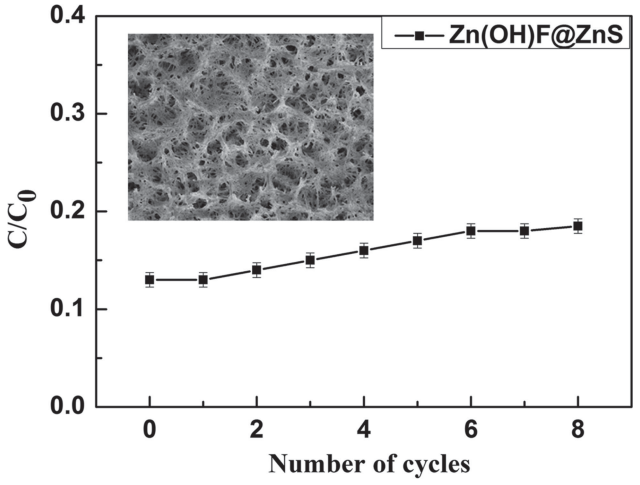


**Figure 6.** Recycling performance of Zn(OH)F@ZnS network-modified capillary microchannels used to continuously adsorb BSA with RT = 10 s. ($C_0$ = 500 μg mL$^{-1}$, the concentration of BSA solution after adsorption was measured every 50 min.) (The inset is the FE-SEM image of the Zn(OH)F@ZnS networks after being continuously used for 400 min.)

### 2.4. Device Fabrication

The large surface-to-volume ratio of the modified networks implied that more proteins would bind to the networks than

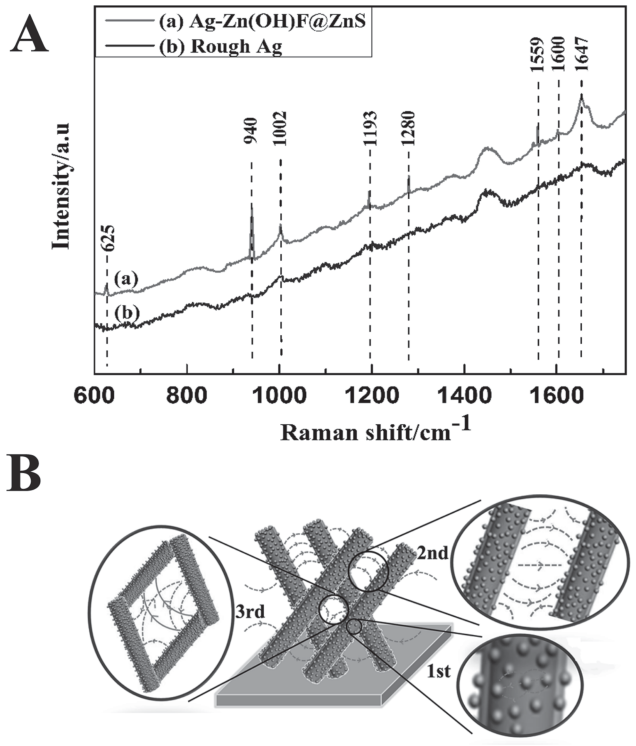


**Figure 7.** A) SERS after BSA solution (20 μL, 1 pM) was injected into the Ag-Zn(OH)F@ZnS network and rough Ag substrates modified microchannel B) Schematic diagrams of the 3D SERS mechanism.

to an unmodified microchannel. Although albumin bound to networks has been successfully isolated by centrifugation, gel filtration, magnetic separation, and membrane-based static microfiltration, there are obvious nuances and specific limitations with each method.[24] In centrifugation, the outcome can be affected by washing duration, solution volume, and protein content and aggregation, and care must be taken to ensure that no false results are obtained.[25] Compared with the above traditional methods to trap and detect albumin, a device based on 3D nest-like network-modified microchannels, such as that depicted in **Figure 8**A, could not only allow continuous high-throughput separation of proteins from large volumes of complex biological matrices, but could also offer a new route to detect proteins by direct examination of the protein-coated material surface. Furthermore, during the enrichment process in the 3D network-modified capillary microchannels, the integration of micro- and nanofluid volumes achieved high enrichment efficiency because of the micro- and nanopores in the network, respectively.

To show the practical applications of the 3D network-modified microchannels, Ag-Zn(OH)F@ZnS network-modified capillary microchannels were sandwiched between two polydimethylsiloxane (PDMS) slices, as shown in Figure 8B. The enrichment performance using an original BSA concentration of 50 μg $mL^{-1}$ was tested using normal and bent configurations, as shown in Figure 8C. Under the same conditions, the specific enrichment performance of the 3D network-modified microdevice decreased by only 2% when bent compared with that when flat. To further explore the structural stability of the microdevice, its recycling enrichment performance was also tested, as shown in Figure 8D. The bent microdevice was evaluated by continuously using Ag-Zn(OH)F@ZnS network-modified capillary microchannels to adsorb 50 μg $mL^{-1}$ BSA solution for 20 s and measuring the exit BSA concentration every 50 min. $C/C_0$ increased slightly with the duration of fluid flow. After 400 min, the BSA adsorption performance of the bent microdevice was similar to that of the flat microdevice, which indicated that the fabricated 3D network exhibits high stability in its standard liquid contact medium. These results revealed

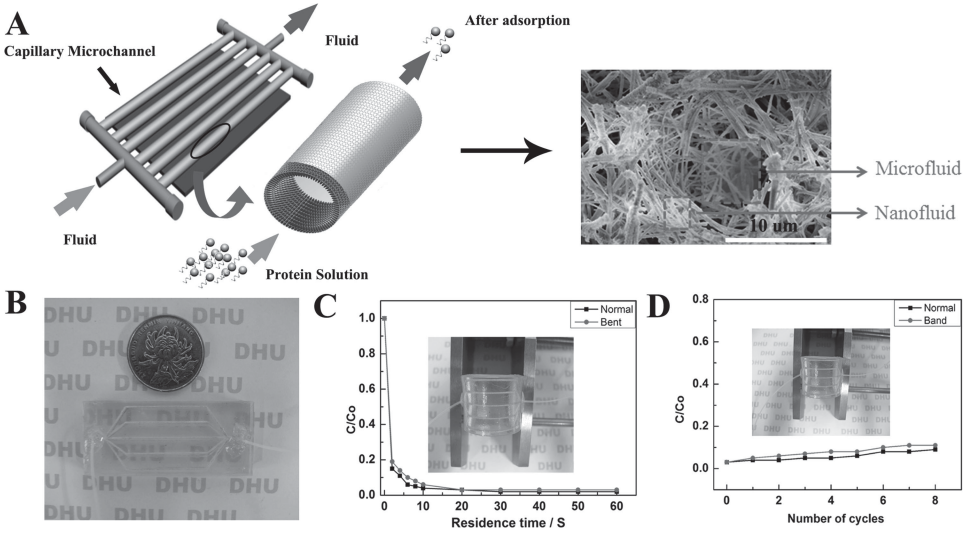


**Figure 8.** A) Prototype device containing multiple Ag-Zn(OH)F@ZnS network-modified capillary microchannels for continuous protein enrichment. Photographic images of B) the fabricated microdevice, C) comparison of BSA enrichment performance from a concentration of 50 μg $mL^{-1}$ for the flexible microdevice tested as normal and bent, and D) comparison of recycling performance for continuous BSA enrichment for bent and flat microdevices.

the potential of the fabricated flexible microdevice in practical applications. The transparent flexible microdevice also showed great potential for online SERS detection of trace biomolecules.

## 3. Conclusions

A microfluidic platform based on 3D stable nest-like networks in confined microchannels was fabricated via a facile, template-free, continuous fluid construction method. The 3D networks consisted of micro/nanoporous structures with large surface areas and could be modified easily. The networks exhibited excellent structural stability performance, which was supported by FEA simulation and recycle adsorption experiments. Multifunctional networks were fabricated by in situ chemical conversion with TAA, and Ag NPs using the original network as a template. The results indicated that our wet-chemical fluid-construction method provides a low-cost, facile and feasible approach to integrate stable 3D networks into confined microfluidic channels for the first time, and could be adapted to generate other multifunctional structures.

The novel 3D structure integrated with microfluidic technology readily captured biomolecules because of its large effective reaction surface area, achieving rapid, high-throughput and continuous adsorption compared with the traditional methods. In addition, the integration of Ag decorated 3D stable networks into the microdevice exhibited excellent trace (1 pM) biomolecule SERS detection ability, owing to their unique 3D network structure and three kinds of hot spots in a large 3D volume. The flexible integrated device not only realized continuous recycling high-throughput separation of proteins from large volumes of complex biological matrices, but also exhibited great potentials in online SERS detection. As demonstrated for the capture and detection of biomolecules, this type of functional stable 3D network provided a new design for microfluidic systems suitable for a variety of biomedical, environment and energy-harvesting applications.

## 4. Experimental Section

*Reagents and Materials*: BSA was purchased from Sigma-Aldrich (St. Louis, MO, USA). All other chemicals and reagents were purchased in the highest grade commercially available and used without further purification. Aqueous solutions were prepared with ultrapure water (UPW, 18.2 MΩ cm) obtained from a Milli-Q water purification system (Millipore Corp., Bedford, MA, USA) unless stated otherwise. Silica glass capillaries (GL Sciences, Inc., Japan) with an internal diameter (i.d.) of 530 μm and a polyimide outer coating were used as microchannels. The inner surfaces of the capillary microchannels were successively rinsed with concentrated sulfuric acid/peroxide/UPW (v/v/v, 4:1:20; 130 °C), UPW, ammonia/peroxide/UPW (v/v/v, 1:4:20; 70 °C), and UPW and then dried in an oven.

*Fabrication of Zn(OH)F Nest-Like Networks in Confined Microchannels*: Zn(OH)F nest-like networks were prepared in confined microchannels through a simple two-step process. First, ZnO nanoseeds were fabricated on the inner walls of the microchannels. Solutions of zinc acetate (0.01 M) in ethanol and NaOH (0.04 M) in ethanol were drawn into two syringes (10 mL) that were attached to a dual-syringe infusion pump (Model 22, Harvard Apparatus, USA) and connected by two pinheads to a prefabricated 'Y' pattern formed using Teflon tubes. The 'Y' pattern Teflon tubes were attached to the capillary microchannel with epoxy resin in advance. The silica glass microchannels were then filled with solution as the pump drove the solutions through the 'Y' pattern Teflon tubes at a set rate of 100 μL $min^{-1}$. When the capillary microchannel was full, the pump was stopped and the capillary microchannel was placed in a conventional oven at 60 °C for 4 h. The capillary microchannel was then annealed at 150 °C to ensure uniform adhesion of ZnO nanocrystals to the inner walls of the microchannels. Second, Zn(OH)F nest-like networks were prepared at 90 °C by replacing the two previous solutions with aqueous solutions of zinc nitrate (0.05 M) and ammonium fluoride (0.05 M) in the capillary microchannel over 1.5 h at a pump rate of 25 mL $min^{-1}$. The reaction schematic diagram of the experimental setup was shown in Figure 1A. After the reaction was complete, the capillary microchannel was cleaned with distilled water and dried.

*Preparation of ZnS-Coated Zn(OH)F (Zn(OH)F@ZnS) Nest-like Networks in Confined Microchannels*: Briefly, Zn(OH)F@ZnS nest-like networks were prepared by exposing Zn(OH)F surfaces to a sulfur compound, TAA, by pumping aqueous TAA solution (0.2 M) from two syringes into a capillary microchannel containing prefabricated Zn(OH)F nest-like networks at a rate of 25 μL $min^{-1}$ in a conventional oven at 90 °C for 3 h. The final products were washed with UPW and then dried at 70 °C before the next reaction step.

*Preparation of Ag-Decorated ST-Capped Zn(OH)F@ZnS (Ag-Zn(OH)F@ZnS) Nest-Like Networks in Confined Microchannels*: ST-capped Zn(OH)F@ZnS nest-like networks on the inner walls of microchannels were produced by pumping ST (0.2 M) from two syringes into a capillary microchannel containing Zn(OH)F@ZnS networks at a rate of 25 μL $min^{-1}$ for 2 h, followed by washing and drying. Colloidal Ag was prepared by reducing $AgNO_3$ with $NaBH_4$ according to the procedure described by Vlčková *et al*.[26] Briefly, $AgNO_3$ solution (15 mL, 0.0025 M) was added at a rate of 1.8 mL $min^{-1}$ at 4 °C to an aqueous solution of $NaBH_4$ (0.0075 g, 150 mL). The Ag colloid was then pumped from two syringes into a capillary microchannel containing ST-capped Zn(OH)F@ZnS networks at a rate of 10 μL $min^{-1}$ for 1 h. The capillary microchannel was then dried at 60 °C.

*Characterization of Nest-Like Networks in Confined Microchannels*: Field emission scanning electronic microscope (FE-SEM) images were taken on an S-4800 FE-SEM (Hitachi, Ltd., Japan) to characterize networks morphology. FE-SEM samples were prepared by cutting subject capillaries into pieces. Transmission electron microscope (TEM) and high-resolution transmission electron microscope (HRTEM) images were obtained with a JEM-2100F TEM (JEOL, Ltd., Japan, 200 kV). Energy-dispersive X-ray (EDX) analyses were also performed during TEM examinations. Samples for TEM and HRTEM analyses were prepared by scraping and collecting networks from the inner walls of microchannels on which networks had been grown. X-ray photoelectron spectroscopy (XPS) was performed using a PHI 5000 versaprobe scanning ESCA microprobe (Ulvac-PHI, Ltd., Japan).

*Capture and Detection of Biomolecules (BSA) Through the Nest-like Network-Modified Flexible Microfluidic Device*: All networks were modified with ST for BSA enrichment and detection, which were produced by pumping 0.2 M ST from two syringes into a capillary microchannel containing various networks at a rate of 25 μL $min^{-1}$ for 2 h, followed by washing and drying. Appropriate amounts of BSA were dissolved in 0.5% NaCl aqueous solution to give desired concentrations (50, 200, 500, and 1000 μg $mL^{-1}$) and then directed through various networks modified microchannels with various residence times (RT). The adjustment of residence time was realized by changing the pumping speed of the BSA solution. Determination of BSA concentration at the exit was performed by the bicinchoninic acid (BCA) method using an Enhanced BCA Protein Assay Kit (Beyotime, Jiangsu, China). The enrichment capacity was monitored by measuring the absorption with a Lambda 35 ultraviolet–visible (UV–vis) absorption spectrophotometer (PerkinElmer, USA). The durability of a single modified microchannel was also investigated by continuously using it at the optimum RT for efficient BSA trapping. The ability of the modified microchannels to detect BSA was tested by introducing 1 pM BSA into microchannels with Ag-Zn(OH)F@ZnS networks and assessed by SERS. A Jobin Yvon micro-Raman spectroscope (Super LabRam, Horiba, Ltd., Edison, NJ, USA) equipped

with an integral Olympus BX40 microscope with 50× or 10× objective (8 mm), holographic grating (1800 g $mm^{-1}$), notch filter to remove Rayleigh line, semiconductor-cooler, and 1024 × 256 pixel charge-coupled device detector was introduced to obtain Raman spectra. A 632.8 nm He-Ne laser powered at 5 mW was introduced as an excitation source. Each spectrum was the accumulation of five measurement cycles, and the acquisition time in each case was typically 10 s.

## Supporting Information

Supporting Information is available from Wiley Online Library or from the author.

## Acknowledgements

The authors gratefully acknowledge the financial support by Natural Science Foundation of China (No. 51072034, 51172042), Specialized Research Fund for the Doctoral Program of Higher Education (20110075130001), Science and Technology Commission of Shanghai Municipality (12nm0503900, 13JC1400200), the Program for Professor of Special Appointment (Eastern Scholar) at Shanghai Institutions of Higher Learning, Innovative Research Team in University (IRT1221), Doctor Innovation Program of Donghua University (CUSF-DH-D-2013002) and the Program of Introducing Talents of Discipline to Universities (No.111–2–04).

Received: June 6, 2013
Revised: July 19, 2013
Published online: September 23, 2013

[1] a) J. Zhang, R. J. Coulston, S. T. Jones, J. Geng, O. A. Scherman, C. Abell, *Science* **2012**, *335*, 690; b) T. Harada, D. E. Discher, *Nature* **2011**, *471*, 172; c) P. N. Nge, C. I. Rogers, A. T. Woolley, *Chem. Rev.* **2013**, *113*, 2550; d) L. Gervais, N. D. Rooij, E. Delamarche, *Adv. Mater.* **2011**, *23*, H151; e) D. Mark, S. Haeberle, G. Roth, F. V. Stettenz, R. Zengerle, *Chem. Soc. Rev.* **2010**, *39*, 1153; f) Y. Sameenoi, K. Koehler, J. Shapiro, K. Boonsong, Y. L. Sun, J. Collett, J. Volckens, C. S. Henry, *J. Am. Chem. Soc.* **2012**, *134*, 10562.

[2] a) I. Lee, Y. Yoo, Z. Cheng, H. K. Jeong, *Adv. Funct. Mater.* **2008**, *18*, 4014; b) C.-H. Choi, D. A. Weitz, C.-S. Lee, *Adv. Mater.* **2013**, DOI: 10.1002/adma.201204657; c) M. I. Bodnarchuk, L. Li, A. Fok, S. Nachtergaele, I. F. Ismagilov, D. V. Talapin, *J. Am. Chem. Soc.* **2011**, *133*, 8956; d) Y. Elani, A. J. deMello, X. Niu, O. Ces, *Lab Chip* **2012**, *12*, 3514; e) S. Marre, K. F. Jensen, *Chem. Soc. Rev.* **2010**, *39*, 1183; f) J.-H. Kang, E. Reichmanis, *Angew. Chem. Int. Ed.* **2012**, *51*, 11841.

[3] a) M. F. El-Kady, R. B. Kaner, *Nat. Commun.* **2013**, *4*, 1475; b) T. Krupenkin, J. A. Taylor, *Nat. Commun.* **2012**, *2*, 448; c) M. Xue, Z. Xie, L. Zhang, X. Ma, X. Wu, Y. Guo, W. Song, Z. Li, T. Cao, *Nanoscale* **2011**, *3*, 2703; d) E. Kjeang, R. Michel, D. A. Harrington, N. Djilali, D. Sinton, *J. Am. Chem. Soc.* **2008**, *130*, 4000; e) R. S. Jayashree, L. Gancs, E. R. Choban, A. Primak, D. Natarajan, L. J. Markoski, P. J. A. Kenis, *J. Am. Chem. Soc.* **2005**, *127*, 16758.

[4] a) C. Franco, H. Gerhardt, *Nature* **2012**, *488*, 465; b) I. S. Park, K. Eom, J. S. Son, W.-J. Chang, K. Park, T. Kwon, D. S. Yoon, R. Bashir, S. W. Lee, *ACS Nano* **2012**, *6*, 8665; c) F. Shen, B. Sun, J. E. Kreutz, E. K. Davydova, W. B. Du, P. L. Reddy, L. J. Joseph, R. F. Ismagilov, *J. Am. Chem. Soc.* **2011**, *133*, 17705; d) S. K. Hoi, X. Chen, V. S. Kumar, S. Homhuan, C. H. Sow, A. A. Bettiol, *Adv. Funct. Mater.* **2011**, *21*, 2847; e) P. Yager, T. Edwards, E. Fu, K. Helton, K. Nelson, M. R. Tam, B. H. Weigl, *Nature* **2006**, *442*, 412.

[5] a) Q. Shen, L. Xu, L. Zhao, D. Wu, Y. Fan, Y. Zhou, W.-H. OuYang, X. Xu, Z. Zhan, M. Song, T. Lee, M. A. Garcia, B. Xiong, S. Hou, H.-R. Tseng, X. Fang, *Adv. Mater.* **2013**, DOI: 10.1002/adma.201300082; b) J. Seo, T. J. Lee, S. Ko, H. Yeo, S. Kim, T. Noh, S. Song, M. M. Sung, H. Lee, *Adv. Mater.* **2012**, *24*, 1975; c) H. Wei, B. Chueh, H. Wu, E. W. Hall, C.-W. Li, R. Schirhagl, J.-M. Lin, R. N. Zare, *Lab Chip* **2011**, *11*, 238; d) D. Yang, X. Niu, Y. Liu, Y. Wang, X. Gu, L. Song, R. Zhao, L. Ma, Y. Shao, X. Jiang, *Adv. Mater.* **2008**, *20*, 4770.

[6] a) A. D. Stroock, S. K. W. Dertinger, A. Ajdari, I. Mezic, H. A. Stone, G. M. Whitesides, *Science* **2002**, *295*, 647; b) S. M. Kim, S. H. Lee, K. Y. Suh, *Lab Chip* **2008**, *8*, 1015; c) S. Zheng, E. Ross, M. A. Legg, M. J. Wirth, *J. Am. Chem. Soc.* **2006**, *128*, 9016; d) P. Li, Y. Gao, D. Pappas, *Anal. Chem.* **2011**, *83*, 7863.

[7] a) S. Cheng, Z. Wu, *Lab Chip* **2012**, *12*, 2782; b) J. S. Swensen, Y. Xiao, B. S. Ferguson, A. A. Lubin, R. Y. Lai, A. J. Heeger, K. W. Plaxco, H. T. Soh, *J. Am. Chem. Soc.* **2009**, *131*, 4262.

[8] a) S. Nagrath, L. V. Sequist, S. Maheswaran, D. W. Bell, D. Irimia, L. Ulkus, M. R. Smith, E. L. Kwak, S. Digumarthy, A. Muzikansky, P. Ryan, U. J. Balis, R. G. Tompkins, D. A. Haber, M. Toner, *Nature* **2007**, *450*, 1235; b) C. G. Li, K. Lee, C. Y. Lee, M. Dangol, H. Jung, *Adv. Mater.* **2012**, *24*, 4583.

[9] a) H. Wang, X. Li, H. Nakamura, M. Miyazaki, H. Maeda, *Adv. Mater.* **2002**, *14*, 1662; b) X. Li, H. Wang, K. Inoue, M. Uehara, H. Nakamura, M. Miyazaki, E. Abe, H. Maeda, *Chem. Commun.* **2003**, *8*, 964; c) Z. He, Q. Zhang, Y. Li, H. Wang, *Appl. Catal. B: Environ.* **2010**, *93*, 376; d) Z. He, Q. Zhang, H. Wang, Y. Li, *Biomed. Microdevices* **2011**, *13*, 865.

[10] a) L. Jiang, M. Zhang, J. Li, W. Wen, J. Qin, *Adv. Mater.* **2012**, *24*, 2191; b) J. Park, S. Wang, M. Li, C. Ahn, J. K. Hyun, D. S. Kim, D. K. Kim, J. A. Rogers, Y. Huang, S. Jeon, *Nat. Commun.* **2012**, *3*, 916; c) M. Jamal, A. M. Zarafshar, D. H. Gracias, *Nat. Commun.* **2011**, *2*, 527; d) H. Liu, R. M. Crooks, *J. Am. Chem. Soc.* **2011**, *133*, 17564; e) H. Wu, T. W. Odom, D. T. Chiu, G. M. Whitesides, *J. Am. Chem. Soc.* **2003**, *125*, 554.

[11] a) Y. Wang, Y. Liu, Y. Cheng, E. Kim, G. W. Rubloff, W. E. Bentley, G. F. Payne, *Adv. Mater.* **2011**, *23*, 5817; b) P. Lin, X. Luo, I.-M. Hsing, F. Yan, *Adv. Mater.* **2011**, *23*, 4035; c) U. Dharmasiri, M. A. Witek, A. A. Adams, J. K. Osiri, M. L. Hupert, T. S. Bianchi, D. L. Roelke, S. A. Soper, *Anal. Chem.* **2010**, *82*, 2844.

[12] a) K. Wang, J. Chen, Z. Zeng, J. Tarr, W. Zhou, Y. Zhang, Y. Yan, C. Jiang, J. Pern, A. Mascarenhas, *Appl. Phys. Lett.* **2010**, *96*, 123105; b) C. Zhu, D. Zhao, J. Chen, Y. Li, L. Wang, L. Wang, Y. Zhou, S. Zhuo, Y. Wu, *Anal. Bioanal. Chem.* **2004**, *378*, 811; c) M. Gonzalez-Bejar, M. Frenette, L. Jorge, J. C. Scaiano, *Chem. Commun.* **2009**, *22*, 3202.

[13] a) A. F. Chrimes, K. Khoshmanesh, P. R. Stoddart, A. Mitchell, K. Kalantarzadeh, *Chem. Soc. Rev.* **2013**, DOI: 1039/C3C35515B; b) X. Lu, D. R. Samuelson, Y. Xu, H. Zhang, S. Wang, B. A. Rasco, J. Xu, M. E. Konkel, *Anal. Chem.* **2013**, *85*, 2320.

[14] M. Lee, K. Lee, K. H. Kim, K. W. Oh, J. Choo, *Lab Chip* **2012**, *12*, 3720.

[15] L. X. Quang, C. Lim, G. H. Seong, J. Choo, K. J. Dob, S. K. Yoob, *Lab Chip* **2008**, *8*, 2214.

[16] S. Lee, M. G. Hahm, R. Vajtai, D. P. Hashim, T. Thurakitseree, A. C. Chipara, P. M. Ajayan, J. H. Hafner, *Adv. Mater.* **2012**, *24*, 5261.

[17] a) G. N. R. Tripathi, M. J. Clements, *Phys. Chem. B* **2003**, *107*, 11125; b) S. W. Joo, S. W. Han, K. Kim, *Langmuir* **2000**, *16*, 5391.

[18] M. Kurylowicz, M. Giuliani, J. R. Dutcher, *ACS Nano* **2012**, *6*, 10571.

[19] a) A. R. Brandao, H. S. Barbosa, M. A. Z. Arruda, *J. Proteomics* **2010**, *73*, 1433; b) M. Weinkauf, G. Hutter, Y. Zimmermann, E. Hartmann,

A. Rosenwald, M. Dreyling, *Talanta* **2010**, *80*, 1539; c) D. E. Sleat, H. Lackland, Y. Wang, I. Sohar, G. Xiao, H. Li, P. Lobel, *Proteomics* **2005**, *5*, 1520; d) M. He, A. E. Herr, *Anal. Chem.* **2009**, *81*, 8177.

[20] J. Kneipp, H. Kneipp, K. Kneipp, *Chem. Soc. Rev.* **2008**, *37*, 1052.

[21] C. Sun, X. Wu, H. Ding, L. Zhao, F. Wang, J. Yang, X. Liu, *J. Fluoresc.* **2009**, *19*, 111.

[22] a) D. L. Phillips, X. Jie, H. Liu, C. K. Chong, H. Corke, *Anal. Lett.* **1999**, *32*, 2703; b) E. Podstawka, G. Niaura, L. M. Proniewicz, *J. Phys. Chem. B* **2010**, *114*, 1010; c) I. R. Vassiliev, A. R. Offenbacher, B. A. Barry, *J. Phys. Chem. B* **2005**, *109*, 23077; d) M. Xu, V. Shashilov, I. K. Lednev, *J. Am. Chem. Soc.* **2007**, *129*, 11002.

[23] C. R. Jacob, S. Luber, M. Reiher, *Chem.-Eur. J.* **2009**, *15*, 13491.

[24] a) H. Kawasaki, T. Akira, T. Watanabe, K. Nozaki, T. Yonezawa, R. Arakawa, *Anal. Bioanal. Chem.* **2009**, *395*, 1423; b) L. Lartigue, C. Wilhelm, J. Servais, C. Factor, A. Dencausse, J.-C. Bacri, N. Luciani, F. Gazeau, *ACS Nano* **2012**, *6*, 2665; c) L. Qing, Y. Xue, Y. Zheng, J. Xiong, X. Liao, L. Ding, B. Li, Y. Liu, *J. Chromatogr. A* **2010**, *1217*, 4663; d) K. Thode, M. Lück, W. Semmler, R. H. Müller, M. Kresse, *Pharm. Res.* **1997**, *14*, 905.

[25] P. Aggarwal, J. B. Hall, C. B. McLeland, M. A. Dobrovolskaia, S. E. McNeil, *Adv. Drug Delivery Rev.* **2009**, *61*, 42.

[26] B. Vlčková, P. Matějka, J. Šimonová, K. Čermáková, P. Pančoška, V. J. Baumruk, *Phys. Chem.* **1993**, *97*, 9719.